Charge Diagnostics for Laser Plasma Accelerators

K. Nakamura, A. J. Gonsalves, C. Lin, T. Sokollik, A. Smith, D. Rodgers, R. Donahue, W. Bryne and W. P. Leemans

Lawrence Berkeley National Laboratory, University of California, Berkeley, CA 94720, USA

Abstract. The electron energy dependence of a scintillating screen (Lanex Fast) was studied with sub-nanosecond electron beams ranging from 106 MeV to 1522 MeV at the Lawrence Berkeley National Laboratory Advanced Light Source (ALS) synchrotron booster accelerator. The sensitivity of the Lanex Fast decreased by 1% per 100 MeV increase of the energy. The linear response of the screen against the charge was verified with charge density and intensity up to 160 pC/mm^2 and 0.4 pC/ps/mm^2, respectively. For electron beams from the laser plasma accelerator, a comprehensive study of charge diagnostics has been performed using a Lanex screen, an integrating current transformer, and an activation based measurement. The charge measured by each diagnostic was found to be within ± 10 %.

Keywords: Laser plasma accelerator, charge diagnostics, Lanex, ICT, activation
PACS: 07.77.Ka, 29.27.Fh, 41.75.Fr, 52.38.Kd, 52.38.Ph

INTRODUCTION

Laser plasma accelerators (LPAs) [1] have shown remarkable progress over the past decade along with the advances in laser technology. In 2006, the production of GeV electron beams was demonstrated in just a few centimeters [2, 3], by using a discharge capillary based guiding structure [4]. Several injection schemes have been proposed to improve stability and quality of e-beams [5, 6, 7], and initial experiments have showed promising results [8, 9, 10]. This progress is making LPAs attractive as a driver for a light source ranging from THz [11] to x-ray [12, 13].

A precise measurement of electron beam (e-beam) charge is essential for any kind of accelerator. Numerous technologies have been studied for LPA produced e-beam charge detection, such as Faraday cups, integrating current transformers (ICTs) [14], activation based measurements [15], imaging plates (IPs), and scintillating screens with cameras. Since an LPA can provide e-beams with a wide range of the energy spread and divergence, a charge diagnostic with imaging capability is desired, leading to detailed studies of the IPs [16, 17, 18] and scintillating screens [19, 20, 21].

Among many kinds of scintillating screens from various manufactures, ones with Terbium doped Gadox (Gd_2O_2S : Tb) as an active layer have been commonly used in the LPA community. The light yield from the screens has been experimentally calibrated against the ICT by using e-beams from rf-accelerator (RFA) with 3 – 8 MeV electron energy [19] and 40 MeV electron energy [21]. By using broadband electron beams from an LPA, sensitivity for 1 to 80 MeV electrons was experimentally calibrated against the IP [20]. Although simulations suggested that the scintillating screens were energy insensitive above a few MeV [19], a detailed experimental study with electrons above 80 MeV has not been reported yet. Since recent progress in the LPA research has pushed attainable energy to a GeV level, it is important to experimentally explore the applicable energy range of the screens above a GeV.

A Faraday cup and ICT have been used as reliable charge diagnostics in the RFA community. Since the Faraday cup has to physically capture electrons, the size can be an issue for high energy e-beams. In contrast, the ICT is a non-destructive, energy independent and compact diagnostic. Despite of all favorable features of the ICT for LPA, its use for LPA produced e-beams has been questioned in recent studies. It was reported in Ref. [19] that the ICT overestimated the e-beam charge by more than a order of magnitude compared to the measurement based on the RFA-calibrated scintillating screen, and the source of discrepancy was attributed to the electromagnetic pulse (EMP) from the laser-plasma interaction. Another cross-calibration using LPA produced e-beams was reported in Ref. [22], where ICT overestimated a factor of about 3 – 4 compared to the IP based charge measurements. Both studies indicated that further cross-calibration measurements and detailed investigations were necessary regarding the use of the ICT in a harsh laser-plasma environment.

In this paper, we have experimentally studied the sensitivity of the scintillating screen (Lanex Fast, Kodak, Rochester, NY, United States) using e-beams provided by the synchrotron booster ring (SBR) accelerator in the Ad-

vanced Light Source (ALS), Lawrence Berkeley National Laboratory (LBNL). The energy of the electron beam was varied from 106 MeV to 1522 MeV covering the unexplored energy range. The linearity of the response against the charge density and charge intensity has been extensively studied as well. The study provides essential information for the Lanex to be a charge diagnostic of LPA produced GeV e-beams. Also described in this paper is the cross-calibration measurements among the ICT, Lanex, and activation based measurement with LPA produced e-beams. The results show that the ICT can be an accurate diagnostic for an LPA.

LANEX CALIBRATION WITH RF-ACCELERATOR

Experimental Setup

The light yield of the Lanex against relativistic mono-energetic electron beams was studied at the booster-to-storage ring (BTS) beamline of the ALS, LBNL. The ALS linear accelerator (Linac) provided 50 MeV e-beams with a micro bunch duration of $\simeq$30 ps in full-width half-maximum (FWHM), and one or two micro bunches with 8 ns separation. The total charge was controlled by changing the bias voltage of the thermionic electron gun (gun bias voltage). The e-beam from the Linac was injected into the SBR accelerator and further accelerated up to 1522 MeV. The e-beam was then extracted from the SBR by the kicker magnet system, a part of which is illustrated in Fig. 1 (a). In normal operation, the kicker system extracted the e-beam at the top of the SBR magnets' current ramp, providing the highest e-beam energy, 1522 MeV. By changing the trigger timing and field strength of the kicker system, an e-beam with lower energy was extracted from the SBR and sent to BTS beamline.

In this paper, two types of Lanex Fast were studied: Lanex Fast Front (thinner) and Lanex Fast Back (thicker). An ICT (ICT-122-070-05:1, Bergoz Instrumentation, Saint Genis Pouilly, France) was used as the reference. Shown in Fig. 1 (b) is the setup for the ICT – Lanex calibration experiment. Electron beams passed through the ICT and Lanex in a vacuum tube. Signals from the ICT were measured by a oscilloscope (TDS 3054B, Tektronix Inc., Beaverton, OR, United States), and the waveform was recorded. The light emitted by the Lanex was measured by a 12-bit charge coupled device (CCD) camera (FLEA-HIBW, Point Grey, Richmond, BC, Canada) with a video lens of focal length 6.4 mm and f-number 1.4. The upstream surface of the Lanex was covered by a $\simeq 40\mu$m thick aluminum foil. Note that the Lanex, CCD camera, video lens, and aluminum foil described here, were employed to realize an identical setup for LPA experiments at LBNL[2, 3].

The longitudinal bunch duration, momentum spread, and transverse emittance of the e-beam evolved during the acceleration at SBR. Although they were not measured during the experiment described in this paper, they were modeled theoreticaly [23]. The longitudinal bunch duration was estimated to be $\simeq$200 ps FWHM for 1522 MeV e-beams. In order to give a conservative estimate to the charge density and charge intensity at the Lanex, bunch duration of 200 ps FWHM was assumed for all the electron energies studied in this paper. The relative root-mean-square (rms) momentum spread of the e-beam was estimated to be $\simeq 4 \times 10^{-3}$ to $\simeq 6.3 \times 10^{-4}$, and e-beams were considered to be mono-energetic.

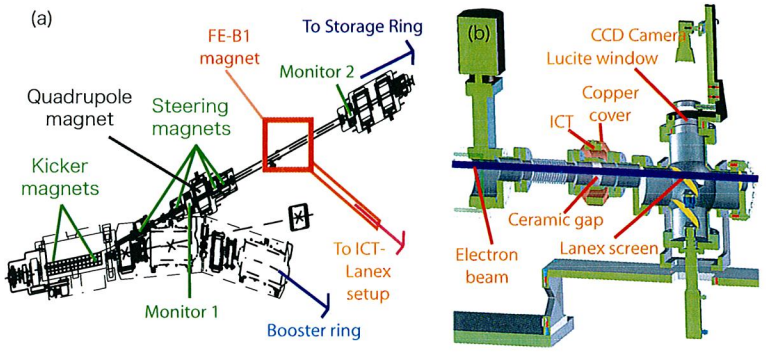

FIGURE 1. (a) Schematic of a part of the booster synchrotron ring accelerator and a part of the booster to storage beamline. (b) Setup for the ICT – Lanex calibration experiment.

Results

The light yield of the Lanex and e-beam charge from the ICT were measured simultaneously for the calibration. For the image processing, there were a couple of effects taken into account: 1) darkening in the edges of acquired images due to the finite collection solid angle, 2) darkening/brightening due to the 45 degree orientation of the Lanex. In order to evaluate those effects, the transverse and longitudinal light location dependences were measured by using a green LED. The measured light location dependences were also used for the relative calibration between this setup and others with different distances [24]. Typical processed images for 1289 MeV and 106 MeV electron energy are shown in Fig. 2 (a) and (b). For a charge measurement by the ICT, the waveform was recorded for each shot, an example of which is shown in Fig. 2 (c). For each shot, the background level was evaluated by averaging signal between 0 ns and the first vertical dotted line, and was indicated by the dashed line. To obtain charge, the signal between the second and third vertical dotted lines was integrated.

Measurements of e-beam charge and light yield from the Lanex Fast Back were conducted for 15 different electron energies with 1 and 2 micro bunch modes. For each experiment, an appropriate ND filter and CCD camera gain were chosen, and more than 100 shots were acquired scanning the gun bias voltage to explore a wide range of the total charge. Shown in Fig. 2 (d) is the CCD camera total count as a function of the measured charge by the ICT for 889 MeV electron energy. The measurements of 1-bunch (circles) and 2-bunch (squares) modes are placed on top of each other. The linear fitting was done for the combined dataset, and the slope (conversion factor) is shown in the inset. To evaluate the quality of the fit, the fit error $\hat{\varepsilon}$ is shown at the lower right box and is defined by the mean of the normalized standard deviation,

$$\hat{\varepsilon} = \frac{1}{g}\sum^{g}\frac{|\mathrm{CCD}_i - f(\mathrm{ICT}_i)|}{f(\mathrm{ICT}_i)}\,, \tag{1}$$

where g is the number of samples, CCD_i and ICT_i are the measured CCD total count and measured charge by the ICT of the i-th sample, and $f(\mathrm{ICT}_i)$ is the total CCD count predicted by the fitting result for the charge measured by the ICT.

The electron energy dependence of the conversion factor is shown in Fig. 2 (e). Shown by the circles are the conversion factors, and by the error bars are $\pm\hat{\varepsilon}$ described by Eq. (1), ranging from 1 % to 8 %. The solid line shows the linear fit result to the energy dependence. Note that the conversion factors were normalized to the one for 1000 MeV from the linear fit. The equation for the fitted line is shown as well, indicating that the Lanex Fast Back was 1.2 % less sensitive for every 100 MeV increase of the electron energy. Shown by the square is the conversion factor of the Lanex Fast Front for 1522 MeV electron energy. The Lanex Fast Back yielded 1.9 times more light than the Lanex Fast Front.

The electron energy dependence of the Lanex light yield was not observed in previous works [19, 20, 21]. Since the previously explored energy range was small enough for the difference to be within the measurement error, the observed energy dependence is not contradictory to them. Although the material used was different, it is noteworthy that the IP showed similar energy dependence as well [16, 17]. There are a few possible scenarios that may explain the observed energy dependence. Relativistic electrons ionize material, exciting a certain level followed by the radiative relaxation. They also produce Bremsstrahlung γ-rays, that can create knock-on electrons which also ionize the material. Since

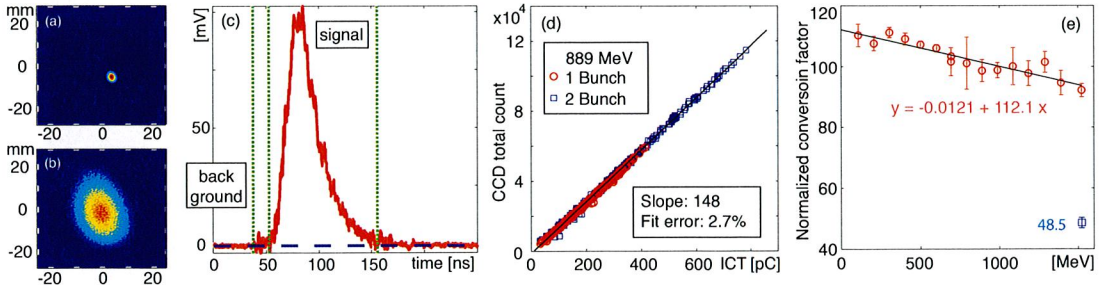

FIGURE 2. (a,b): Typical processed images for (a) 1289 MeV and (b) 106 MeV electron energy. (c): Typical measured ICT signal (solid line). (d): The total CCD count as a function of the charge measured by the ICT for 889 MeV electron energy. (e) The normalized conversion factor as a function of electron energy. See manuscript for descriptions.

higher energy photons get absorbed less in the material [25], the contribution from Bremsstrahlung γ-rays may become less for higher energy electrons. Another possible scenario is that the electron scattering angle is less for higher energy electron, resulting in less interaction with the material.

For all the scans described above, linear relationships were observed between the Lanex light yield and the ICT measured charge. The charge density was explored up to 160 pC/mm^2 in $\sim$ 8 ns for 1391 MeV electron beam with 2 micro bunch mode. With 1 bunch mode, the charge intensity was explored up to 0.4 pC/ps/mm^2. The linear response of the Lanex Fast Back was verified up to those parameters.

CHARGE DIAGNOSTICS CROSS-CALIBRATIONS WITH LASER PLASMA ACCELERATOR

Experimental Setup

Cross-calibrations between the Lanex and ICT, and between the Lanex and activation based method [15] were conducted by using LPA produced e-beams at the LOASIS facility, LBNL [26]. The ICT – Lanex cross-calibration was carried out in the same manner as the calibration with RFA-generated e-beams, which was described in the previous sections. For the Lanex – activation cross-calibration, a target material was irradiated by e-beams for a certain amount of time (typically from 1 to 3 hours), during which the charge was also measured by the Lanex. Based on the total charge measured by the Lanex and the separately measured energy spectrum, a Monte-Carlo simulation was carried out to estimate the activation, which was compared to the measured activation.

The laser that was utilized was the short pulse, high peak power and high repetition rate (10 Hz) Ti:Al_2O_3 laser system. The laser beam was focused by an off-axis parabolic mirror, providing a typical focal spot size $r_0 \simeq 22\,\mu$m with Strehl ratio of 0.7. Here, a Gaussian transverse profile of $I = I_0 \exp(-2r^2/r_0^2)$ is assumed. Full energy and optimum compression gives $P = 31$ TW ($\tau_{in} \simeq 40$ fs FWHM), calculated peak intensity $I_0 = 2P/\pi r_0^2 \simeq 2.8 \times 10^{18}$ W/cm^2, and a normalized vector potential $a_0 \simeq 8.6 \times 10^{-10} \lambda[\mu\text{m}] I^{1/2}[\text{W/cm}^2] \simeq 1.2$.

For the ICT – Lanex calibration, laser pulses were focused onto the downstream edge of a gas jet comprised of 99% helium and 1% nitrogen. The gas jet backing pressure was varied to change charge yield from the LPA. The plasma density was measured by transverse interferometry. The peak plasma density was measured from 3 to 12 $\times 10^{18}$/cm^3, and the longitudinal plasma length was about 0.8 mm. For the Lanex – activation measurement, the laser pulse was focused onto the upstream edge of 100 % helium jet. The peak plasma density was $\sim 8 \times 10^{18}$/cm^3, and plasma longitudinal length was ~ 0.4 mm.

The schematic drawing of the setup is shown in Fig. 3. For the cross-calibrations, the magnet for electron spectrometer was turned off to send e-beams to charge diagnostics. The laser pulse was reflected by the aluminum coated mylar foils toward the laser beam dump. The Lanex Fast Front was placed behind the vacuum window. The upstream surface of the Lanex was covered by a $\simeq 40\mu$m thick aluminum foil. The light from Lanex was observed by an identical CCD camera described in the previous section through the reflection of an aluminum coated 5 μm thick pellicle foil. For the activation measurement, the target was placed behind of the pellicle foil. The target consists of 6 mm thick lead as a γ-ray generator, followed by the 25 mm thick copper as an activation material.

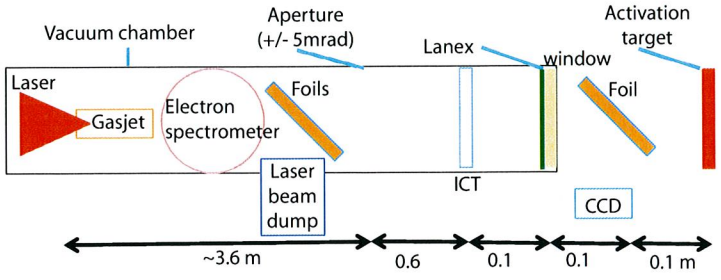

FIGURE 3. Schematic drawing of laser plasma accelerator experiment setup.

Results

Simultaneous measurements of e-beam charge via the ICT and light yield from the Lanex were carried out with LPA produced e-beams. The e-beam energy spectra were measured by a single shot magnetic electron spectrometer [24] before sending the e-beam to charge diagnostics, and broadband e-beams up to 90 MeV of electron energy were observed. Shown in Fig. 4 are (a) a typical measured e-beam on the Lanex , (b) a typical measured ICT signal, and (c) the charge measured by the Lanex versus the charge measured by the ICT. The result showed that the slope for CCD counts – ICT measured charge agreed with the RFA based calibration within ~ 8 % of error. A negative offset, observed from Lanex measured charge, is probably due to the sensitivity of the CCD camera. Note that 0.1 mV offset on the ICT signal gives $\sim$1 pC of error, possibly contributing to the error as well.

The Lanex – activation cross-calibration was conducted separately from the ICT – Lanex cross-calibration. Right before the activation, 50 shots of e-beam energy spectra were taken, and reproducible broadband e-beams up to 250 MeV were observed. A total of 2700 shots was irradiated onto the target in 1 hour, and γ-ray spectroscopy was conducted by using a p-type HPGe detector. The 1345 keV photons from ^{64}Cu decay (half life time 12.7 hour) was used to determine the yield of the isotope. The average production rate was measured to be 9.79×10^6 atoms/minutes. During the activation, the e-beam charge was also measured by the Lanex, giving the average charge of 37 pC/shot. A Monte-Carlo simulation was carried out to estimate isotope production based on the total charge measured by the Lanex and the averaged e-beam energy spectrum. A three dimensional activation distribution in the copper target was calculated, and gave an average production rate of 10.5×10^6 atoms/minutes, agreeing with the experimental results within $\sim 7\%$ of error.

As shown above, Lanex, ICT and activation-based charge diagnostics agreed with each other within ± 10 % of error for LPA produced e-beams. In other words, the ICT measured the LPA-produced e-beam charge within ± 10 % of error, while previous works showed that the ICT overestimated the charge up to two order of magnitudes. It can be explained by the efforts made in our work to minimize the following three possible noise sources of the ICT measurement: (1) EMP from the laser plasma interaction, (2) direct particle/radiation hit on the ICT, and (3) low energy electrons.

There were two kinds of EMP noises observed, one was directly on the scope, and the other was on the cable and/or the ICT. The noise on the scope was separated from the signal in the time domain by extending the cable length. To minimize the noise on the cable, well-shielded cables (Heliax FSJ1-50A, CommScope, Hickory, NC, United States) were employed, and the route of cables was carefully arranged to reduce the noise. Since the higher frequency part of the EMP noise was visible from the waveform, it was used for an indicator while optimizing the route. As can be seen from Fig. 4 (b), the obtained ICT signals did not contain high frequency spikes.

The direct hit of the laser pulse or e-beam onto the ICT can potentially create secondary electrons and/or ionize the material, possibly contributing to the noise. The laser pulse was separated from e-beams to prevent from hitting the ICT. An aperture was utilized for e-beam transverse size to be smaller than the acceptances of the ICT and Lanex, assuring that the e-beams did not hit the ICT or vacuum tube. The ICT was installed outside of the vacuum tube over a ceramic gap so that e-beams propagate in vacuum with minimum disturbance.

The low energy electrons could cause a large discrepancy between the ICT and Lanex measurements because of the following reasons. (1) Non-linear beam size evolution due to the space charge effect can lead to the acceptance mis-match between the two diagnostics. (2) Lanex may not be sensitive to < keV electrons. In this experiment, the ICT

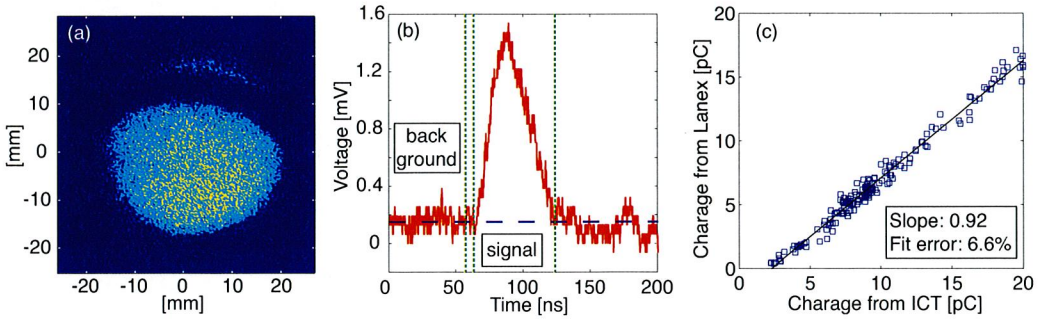

FIGURE 4. (a) Typical measured e-beam profile with Lanex. (b) Typical measured ICT signal (solid line). (c) Lanex measured charge as versus ICT measured charge.

was installed 4.2 m away from the interaction point to assure that the low energy electrons expand enough to minimize their contribution. Furthermore, the small residual magnetic field ($\sim$ 0.4 mT) of the magnetic spectrometer, and the foils used for the laser beam separation may have contributed to eliminate low energy electrons. The distance between ICT and Lanex was kept at a minimum to avoid acceptance mismatch.

Although no quantitative evaluation was performed for each noise source, it was considered to be critical to provide a quiet environment for the charge measurement. Note that the accuracy of the measurement can be improved by a more sensitive camera for Lanex measurements, and by more sensitive electronics for ICT measurements.

CONCLUSIONS

The electron energy dependence of the Lanex Fast light yield was studied from 106 MeV to 1522 MeV e-beams. The Lanex was observed to be 1% less sensitive for every 100 MeV increase in the energy. A comprehensive study of the charge of LPA produced e-beams was conducted, showing that the ICT can provide accurate charge measurement for LPA produced e-beams provided it is used properly. The guideline for the use of the ICT under the harsh LPA environment was discussed.

ACKNOWLEDGMENTS

The authors acknowledge Bas Fleskens, Pablo Gallegos, and Advanced Light Source staff for contribution on the Lanex calibration experiment, Jens Osterhoff, Satomi Shiraishi, Jeroen van Tilborg, Csaba Toth, and Cameron Geddes for their contributions on laser plasma accelerator experiments, and Don Syversrud, Nathan Ybarrolaza, and Zachary Eisentraut for technical support. We also thank Julien Bergoz for the fruitful discussion on the ICT. This work was supported by the U.S. Department of Energy under Contract No. DE-AC02-05CH11231.

REFERENCES

1. E. Esarey, C. B. Schroeder, and W. P. Leemans, *Rev. Mod. Phys.* **81**, 1229–1285 (2009).
2. W. P. Leemans, B. Nagler, A. J. Gonsalves, et al., *Nature Physics* **2**, 696–699 (2006).
3. K. Nakamura, B. Nagler, C. Tóth, et al., *Phys. Plasmas* **14**, 056708 (2007).
4. A. J. Gonsalves, T. P. Rowlands-Rees, B. H. P. Broks, et al., *Phys. Rev. Lett.* **98**, 025002 (2007).
5. E. Esarey, R. F. Hubbard, W. P. Leemans, et al., *Phys. Rev. Lett.* **79**, 2682–2685 (1997).
6. S. Bulanov, N. Naumova, F. Pegoraro, and J. Sakai, *Phys. Rev. E* **58**, R5257–R5260 (1998).
7. E. Oz, S. Deng, T. Katsouleas, P. Muggli, et al., *Phys. Rev. Lett.* **98**, 084801 (2007).
8. C. G. R. Geddes, K. Nakamura, G. R. Plateau, et al., *Phys. Rev. Lett.* **100**, 215004 (2008).
9. J. Faure, C. Rechatin, A. Norlin, A. Lifschitz, Y. Glinec, and V. Malka, *Nature* **444**, 737 – 739 (2006).
10. A. Pak, K. A. Marsh, S. F. Martins, W. Lu, W. B. Mori, and C. Joshi, *Phys. Rev. Lett.* **104**, 025003 (2010).
11. W. P. Leemans, C. G. R. Geddes, J. Faure, et al., *Phys. Rev. Lett.* **91**, 074802 (2003).
12. S. Kneip, S. R. Nagel, C. Bellei, et al., *Phys. Rev. Lett.* **100**, 105006 (2008).
13. M. Fuchs, R. Weingartner, A. Popp, et al., *Nature Physics* **5**, 826 (2009).
14. K. B. Unser, "Design and Preliminary Tests of a Beam Intensity Monitor for LEP," in *Proceedings of the 1989 Particle Accelerator Conference*, IEEE, Piscataway, NJ, 1989, vol. 1, p. 71.
15. W. P. Leemans, D. Rodgers, P. E. Catravas, et al., *Phys. Plasmas* **8**, 2510–2516 (2001).
16. K. A. Tanaka, T. Yabuuchi, T. Sato, et al., *Rev. Sci. Instrum.* **76**, 013507 (2005).
17. N. Nakanii, K. Kondo, T. Yabuuchi, et al., *Rev. Sci. Instrum.* **79**, 066102 (2008).
18. K. Zeil, S. D. Kraft, A. Jochmann, et al., *Rev. Sci. Instrum.* **81**, 013307 (2010).
19. Y. Glinec, J. Faure, A. Guemnie-Tafo, et al., *Rev. Sci. Instrum.* **77**, 103301 (2006).
20. S. Masuda, E. Miura, K. Koyama, and S. Kato, *Rev. Sci. Instrum.* **79**, 083301 (2008).
21. A. Buck, K. Zeil, A. Popp, et al., *Rev. Sci. Instrum.* **81**, 033301 (2010).
22. B. Hidding, G. Pretzler, M. Clever, et al., *Rev. Sci. Instrum.* **78**, 083301 (2007).
23. 1-2 GeV synchrotron radiation source, Tech. Rep. PUB-5172 Rev., Lawrence Berkeley National Laboratory, University of California, Berkeley, CA 94720 (1986).
24. K. Nakamura, W. Wang, N. Ybarrolaza, D. Syversrud, J. Wallig, and W. Leemans, *Rev. Sci. Instrum.* **79**, 053301 (2008).
25. R.-I. I. Corp., Scintillator options for shad-o-box cameras, Tech. Rep. AN-07, Rad-Icon Imaging Corp., www.rad-icon.com, Santa Clara, CA 95054 (2002).
26. http://loasis.lbl.gov.

DISCLAIMER